Estimation and measurement of backscattered signals from pulsed laser radar

Boris Jutzi, Bernd Eberle, Uwe Stilla

FGAN-FOM Research Institute for Optronics and Pattern Recognition
Gutleuthausstr. 1, D-76275 Ettlingen, Germany
Tel: +49 7243 992-337, Fax: +49 7243 992-299, E-mail: boris.jutzi@fom.fgan.de

ABSTRACT

Current pulsed laser radar systems for ranging purposes are based on time-of-flight techniques. Nowadays first pulse as well as last pulse exploitation is used for different application, e.g. urban planning, forestry surveying. Besides this technique of time measurement the complete signal form over the time might be of interest, because it includes the backscattering characteristic of the illuminated field. This characteristic can be used for estimating the aspect angle of a plane with special surface property or estimating the surface property of a plane with a special aspect angle. In this paper a monostatic bi-directional experimental system with a fast digitizing receiver is described. The spatio-temporal beam propagation, the spatial reflectance of the surface, and receiver properties are modeled. A time dependent description of the received signal power is derived and our special surface property is considered. The transversal spatial distribution of the used laser beam was measured and displayed by the beam profile. For a plane surface under various aspect angles the transversal spatial distributions of the beam were simulated and measured. For these angles the corresponding temporal beam distributions were measured and compared with their pulse widths. The pulse spread is used to estimate the aspect angle of the illuminated object. The statistics for different angles was calculated. Different approaches which detect a characteristic time value were compared and evaluated. The consideration of the signal form allows a more precise determination of the time-of-flight. A 3-d visualization of equi-irradiance surfaces allows to assess the spatio-temporal shape of the pulses.

Keywords: remote sensing, pulsed laser radar, signal form analysis, aspect angle, reflection properties

1. INTRODUCTION

The automatic generation of 3-d models for a description of man-made objects (e.g. buildings) is of great interest [Baltsavias et al., 2001]. In photogrammetry a spatial surface is classically determined by triangulation of corresponding image points from two or multiple pictures of the surface. The points are manually searched or automatically calculated by analyzing image structures (e.g. stereo correlation techniques). Besides this indirect measurement using object features which depend on natural illumination, active laser radar systems allow a direct and illumination-independent measurement of the range. The laser radar capture the range information of 3-d objects in a fast, contactless and accurate way. In future applications the efficiency could be increased by analyzing object features.

Unlike the classical radar it is possible to obtain a high lateral geometric resolution since the laser beam divergence is quite small (<1 mrad). In the case of extended objects, which are greater in size than the beam diameter, the characteristical dependence of the received power as a function of the range R is proportional to $1/R^2$ [Jelalian, 1992]. The axial geometric resolution (some cm) depends on the actual status of the temporal signal acquisition and the related applications of the signal processing. A given sampling pattern is used to determine single range measurements. With the given orientation and position of the sensor system in space the measured range information is transformed into 3-d world coordinates.

Laser radar systems can be categorized under different views, e.g. *measurement* technique, *modulation* technique, *detection* technique, or *alignment* technique. Measurement techniques for range determination can be distinguished by the exploited signal properties like phase, frequency, amplitude, time, or a combination of them. Concerning the modulation techniques laser systems can be split in continuous wave (cw) laser or pulsed laser. As detection techniques

direct detection and coherent detection (e.g. heterodyne, homodyne and offset homodyne) are known. According to the alignment of emitter and receiver monostatic and bistatic systems are distinguished. If the emitter and the receiver operate on the same optical axis, the system will be called monostatic, otherwise bistatic. In this contribution we focus on a monostatic pulsed system (direct detection) and the analysis of the signal amplitude.

For applications in remote sensing the pulsed laser with the higher power density compared to cw laser is of advantage, because it allows to operate at long ranges. Pulsed laser radar systems base on time-of-flight ranging techniques to determine the range to the illuminated object. The time-of-flight is measured for the elapsed time between the emitted and backscattered laser pulse. To determine the elapsed time the signal analysis typically operates with an analog threshold detection (e.g. leading edge detection, peak detection, constant fraction detection) [Kamerman, 1993]. The accuracy depends on the reflectivity of the illuminated object [Shapiro et al., 1986]. First pulse as well as last pulse exploitation is used for different applications, e.g. urban planning or forestry surveying, to capture a 3-d scene for a digital terrain model (DTM), digital surface model (DSM), or city model [Stilla & Jurkiewicz, 1999].

Besides this technique of time measurement the complete signal form over the time might be of interest, because it includes the individual characteristics of the illuminated field. The exploitation of the signal form can be used to determine essential object features. For that purpose an advanced range model has to be developed that includes the beam characterization and the surface properties of the illuminated area.

Several spatial models have been proposed to describe the surface properties. One of the first approaches was introduced by Torrance & Sparrow [1967]. The Torrance-Sparrow model describes the radiant intensity reflected from surfaces by a directional distribution. A bi-directional reflectance-distribution function (BRDF) with the general distribution of light within a hemisphere as a function of the angle was introduced by Nicodemus et al. [1977]. Specifications for diffuse surface reflectance of the incident and reflected beam geometry have been shown by Horn & Sjoberg [1979] and upgraded for specular reflectance by Ginneken et al. [1998]. Additionally to these geometrical perspectives physical perspectives were formulated by Nayar et al. [1991]. An overview on backscattering is given by Andrews & Phillips [1998] and a general description of optical scattering is given by Stover [1990].

The studies mentioned above considered the spatial characteristic of the backscattering. The temporal characteristic of the signal at the receiver can be analyzed for measuring the range [Wang & Kostamovaara, 1994]. Delaye & Labeye [2000] exploited the emitted as well as the received digitized pulse for measuring the range. Furthermore, the precise analysis of the temporal signal can be useful to determine scattering properties of the atmosphere [Harms et al., 1978][Walker & McLean, 1999]. Besides the scattering of the atmosphere the backscattering of an objects surface can be explored. The backscattered signal depends on the transversal and longitudinal distribution function of the beam, the object shape function and the BRDF of the surface [Steinvall, 2000]. In other words, with specifications of the linear system theory the object can be seen as a filter convolved with the emitted laser beam. The received signal includes the impulse response of the illuminated object. Investigations on the impulse response of a sphere have been measured by Abrahamsson et al. [1991].

In this paper we investigated the influence of the aspect angle of a plane surface on the spatial and temporal distributions of the laser beam. The investigations were done theoretically and compared with experimentally results. The transversal spatial distribution of the used laser beam was measured and is displayed by the beam profile. For a plane surface under various aspect angles the transversal spatial distributions of the beam were simulated and measured. For these angles the corresponding temporal beam distributions were measured and compared by their pulse width. The pulse spread is used to estimate the aspect angle of the illuminated object. The statistics for different angles is calculated. Different approaches which detect a characteristic time value were compared and evaluated.

2. DESCRIPTION OF THE EXPERIMENTAL SYSTEM

A monostatic bi-directional experimental system has been built-up to analyze the emitted and backscattered short duration laser pulse. The description of the system follows the propagation direction of the pulse. It is schematically illustrated in Fig. 1 and Fig. 2. The system consists of the emitter unit and receiver unit. Additionally the targets are described.

2.1 Emitter unit

We use a Raman shifted Nd:YAG laser that operates at a wavelength of 1543 nm. The pulse energy is 4.2 mJ and the pulse duration at full-width-half-maximum (FWHM) is 2.3 ns. The emitted beam transmits a half-wave plate to convert the vertical linear polarized light into horizontal linear polarized light. The double-concave lens with the negative focal length of 500 mm spreads out the beam divergence to 4 mrad (1/e) and enables a measurable spread of the laser pulse duration. The beam splitter cube I is used to separate the emitted from the received light. The quarter-wave plate converts the linear polarized light into circular polarized light.
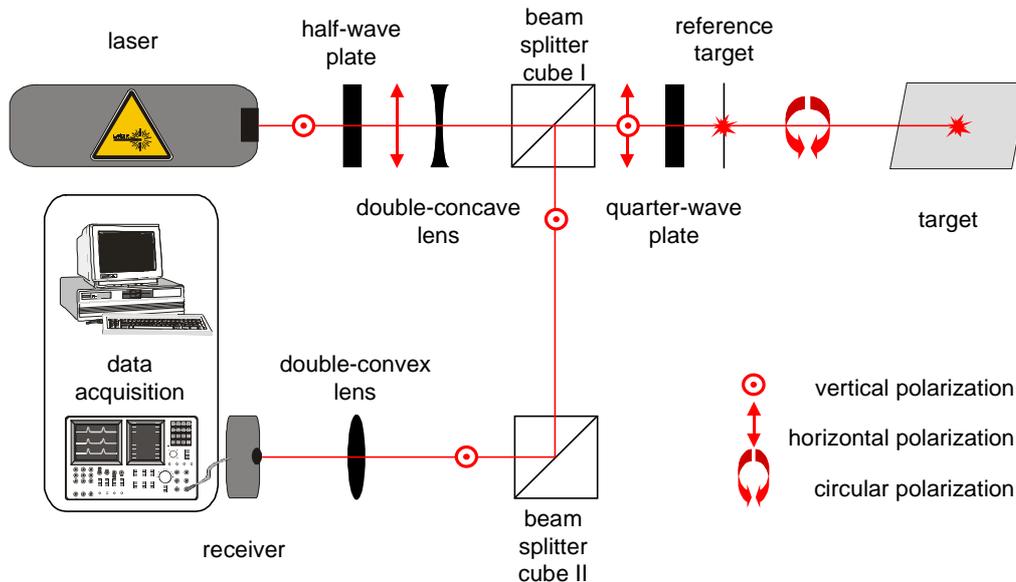
Figure 1: Sketch of the experimental system including emitter unit, receiver unit and targets

2.2 Receiver unit

The received pulse transmits the quarter-wave plate, which converts the polarization state from circular polarization into vertical linear polarization. The beam splitter cube I redirects the beam to the beam splitter cube II, which attenuates the horizontally oriented stray light effected by the emitter unit, and redirects the beam from the environment to a focusing lens. This double-convex lens with the positive focal length of 200 mm focuses the beam to the receiver. The receiver (New Focus 1611-AC) transforms the optical signal into an electrical signal. The receiver detector is a fast InGaAs PIN photodiode with a detector diameter of 100 μm. The photodiode is connected to the receivers preamplifier. The signal is captured with the digital oscilloscope (Tektronix TDS 684A) and the 8-bit data are transferred via analyzer and controller board (National Instruments PCI-GPIB) to a standard PC. The complete electrical system for data acquisition supports at least 1 GHz bandwidth.

2.3 Targets

In order to analyze the received signal waveform the emitted signal waveform has to be know exactly. Since the outgoing pulses show strong variations in the signal amplitude and the signal duration from pulse to pulse, a reference signal waveform of the outgoing pulse is captured for each measurement. An ideal backscattering reference target in form of a thin string is positioned in front of the emitter unit and adjusted in the beam line. Besides this it is possible to calibrate the amplitude of the emitted and received signal power. Thus a critical component for monostatic systems is eliminated.

As target under test we used a diffuse white plate made of synthetic material, with an extension greater than the laser beam width. The plate was mounted on a tripod at a distance of approximately 10 m. The experiment was carried out by rotating the plate in steps of fifteen degrees.
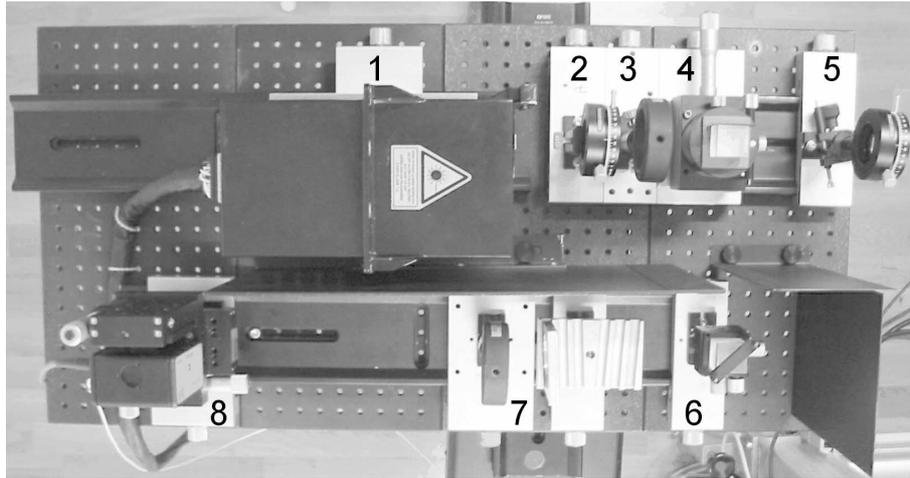
Figure 2: Experimental system. (1) laser, (2) half-wave plate, (3) double-concave lens, (4) beam splitter cube I, (5) quarter-wave plate, (6) beam splitter cube II, (7) double-convex lens, (8) receiver

3. MODELING OF BACKSCATTERED SIGNALS

In this section we derive the illumination of an extended object with a laser beam resulting into a backscattered signal that depends on the geometrical shape of the illuminated surface. Some definitions have to be modified for our purpose: (i) initiate the function of the spatio-temporal distribution to describe the *beam propagation*, (ii) formulate the *geometrical reflectance* of the shape with a hypothetical Lambertian surface, (iii) consider the aperture properties of the *receiver*, (iv) integrate (i-iii) to the *laser radar range equation*, (v) satisfy the experimental assumptions for the *extended object with simplified surface* and (vi) suggest the linear system theory for *system description*.

3.1 Beam propagation

The transmitted laser beam is characterized by the optical power, beam width, beam divergence, transversal intensity profile and direction of propagation. We introduce the distribution function K for a spatial and temporal modeling of the transmitted power P_t. The spatio-temporal distribution function K is normalized and dimensionless. Let us assume K is separable into a transversal spatial distribution function K_t and a longitudinal temporal distribution function K_l. K_t as well as K_l are projections of K. The irradiance E depends on K and can be described as a function of range r, elevation angle ε, azimuth angle α, and time t

$$E(r,\varepsilon,\alpha,t) = P_t \cdot \frac{\eta_{atm}(r)}{4\pi r^2} = P_o \cdot K(r,\varepsilon,\alpha,t) \cdot \frac{\eta_{atm}(r)}{4\pi r^2} = P_o \cdot K_l(t-\frac{r}{c}) \cdot K_t(\varepsilon,\alpha) \cdot \frac{\eta_{atm}(r)}{4\pi r^2} . \tag{1}$$

P_o is the output power, c is the speed of light and the irradiance is spread proportionally to $1/(4\pi r^2)$. The atmospheric attenuation η_{atm} with attenuation coefficient λ_a is

$$\eta_{atm}(r) = \exp(-\frac{r}{\lambda_a}) . \tag{2}$$

Assuming a Gaussian distribution for K_l and an exponential function as an approximation for K_t we obtain with the constants k_1, k_2, k_3, k_4:

$$K_l(t-\frac{r}{c}) = k_1 \cdot t^2 \cdot \exp(-k_2 \cdot t) \quad \text{and} \quad K_t(\varepsilon,\alpha) = k_3 \cdot \exp(-k_4 \cdot (\varepsilon^2 + \alpha^2)) . \tag{3}$$

3.2 Geometrical reflectance

Let us further assume that the object extent is greater than the laser beam width. For such an extended target the total hemispherical reflectance of a target is given with ρ. The target reflectance is often assumed to be uniform and with an isotropic surface, also known as Lambertian diffuser. This is an often used approximation for the illuminated surface to avoid the complicated distribution function. The general distribution of light within a hemisphere as a function of angle is called BRDF. The BRDF is a measure for the quantity of light, incident with an arbitrary direction on a surface or medium and reflected into an arbitrary direction into the hemisphere. For a monostatic system the angle of the incident and reflected light coincides and effects in a simplified distribution function, but is still related to angle of incidence. With the assumption of a uniform reflectance property of the surface the target reflectance $\rho_{geo}(r,\varepsilon,\alpha)$ depends only on the geometrical shape.

3.3 Receiver

The receiver attenuates the perceived radiant intensity which is described by S and depends on the aperture diameter D and range r. Assuming $D << r$ the receiver characteristic with η_{sys} as system attenuation is given by

$$S(D,r) = \frac{\pi \cdot D^2}{4 \cdot \pi \cdot r^2} \cdot \eta_{sys} . \tag{4}$$

3.4 Laser radar range equation

The components mentioned above are integrated with respect to the two-way time of flight

$$P_r = \int_0^\infty \int_{-\pi/2}^{\pi/2} \int_0^{2\pi} P_o \cdot K(2r,\varepsilon,\alpha,t) \cdot \frac{\eta_{atm}(2r)}{4\pi r^2} \cdot \rho_{geo}(r,\varepsilon,\alpha) \cdot S(D,r) \cdot r^2 \cdot \cos(\varepsilon) \, d\alpha \, d\varepsilon \, dr , \tag{5}$$

where P_r is the received signal power. As general expression we get

$$P_r = P_o \cdot \frac{D^2}{16 \cdot \pi} \cdot \eta_{sys} \cdot \int_0^\infty K_l(t - \frac{2r}{c}) \cdot \frac{\eta_{atm}(2r)}{4\pi r^2} \int_{-\pi/2}^{\pi/2} \cos(\varepsilon) \int_0^{2\pi} K_t(\varepsilon,\alpha) \cdot \rho_{geo}(r,\varepsilon,\alpha) \, d\alpha \, d\varepsilon \, dr . \tag{6}$$

3.5 Extended object with simplified surface

For an extended object with simplified surface in form of a plane plate several assumptions are essential: We neglect the system relevant attenuation, and assume a stationary target and a stationary radar system. Consider the range R is related to the beam radius b with $R >> b$, the reflectance of the plane plate can be described with

$$\rho_{geo}(r,\varepsilon,\alpha) = \rho(\varphi) \cdot \delta(r,R), \tag{7}$$

where δ is the delta function and φ is the angle between the optical axis and the normal of the plate. Hence the received power of an extended object with simplified surface is

$$P_r(t) = P_o \cdot \frac{D^2}{4 \cdot R^2} \cdot K_l(t - \frac{2R}{c}) \cdot \eta_{atm}(2R) \cdot \rho(\varphi), \tag{8}$$

where the received signal is a function of the temporal distribution function and to the aspect angle of the plate.

3.6   System description

Assuming linear properties the linear system theory is helpful to describe the system. It is easy to represent the output signal $y(t)$ as a convolution of the input signal $x(t)$ with the system function $s(t)$:

$$y(t) = s(t) \otimes x(t) . \tag{9}$$

In our system the input signal $x(t)$ is the temporal distribution function of the emitted pulse, the system function $s(t)$ is the target reflectance, and the output signal $y(t)$ is the received pulse. When we choose $\delta_0(t)$ (Dirac delta function) as input function $x(t)$, we will obtain

$$s(t) = h(t) \quad \text{for} \quad x(t) = \delta_o(t) . \tag{10}$$

That means, the impulse response $h(t)$ determines the system properties. For determination of the system properties by $h(t)$ we assume a Dirac delta function. In practice the realization of an ideal pulse is difficult.

4.   EXPERIMENTS

Subject of experimental investigations is to determine the aspect angle of an extended object with simplified surface. The object is illuminated with a laser pulse. The experiments can be distinguished concerning spatial (transversal) and temporal (longitudinal) evaluation.

4.1   Spatial evaluation

The spatial distribution of the beam is often approximated by a Gaussian distribution or for analytical purposes by a band limited Uniform distribution. For many applications these assumptions are sufficient. In Eq. 6 we derive the function of the spatial distribution which effects the received signal power. For this purpose it is essential to measure the spatial distribution. For measurement 600 single shots of the pulsed laser system were directed to the plate (see Section 2.3). The surface radiance of the plate was digitally captured. The propagation direction of the beam was perpendicular to the surface.
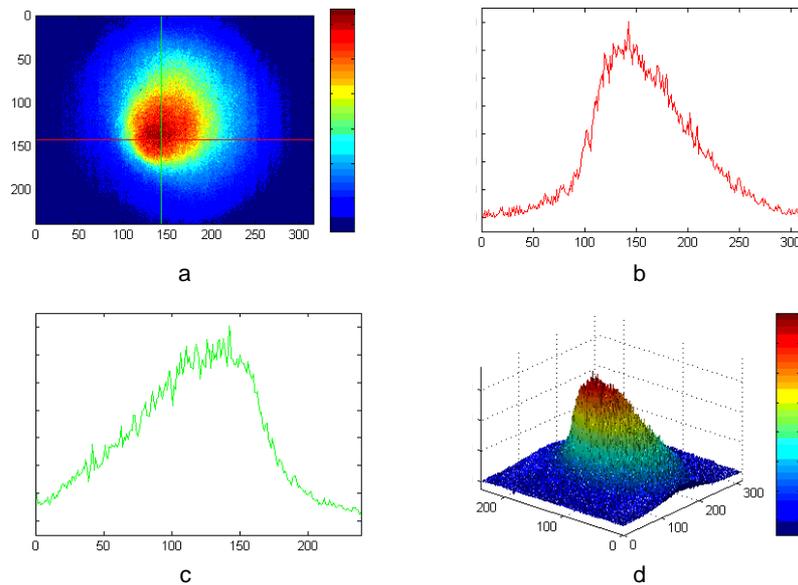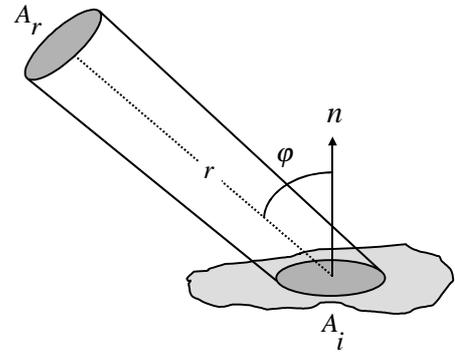

Figure 3: Measured distribution of the beam. a) 2-d visualization, maximum intensity indicated by row and column, b) distribution of row, c) distribution of column, d) 3-d visualization.

For data acquisition we used an IR-camera (900-1700 nm) with an InGaAs CCD chip (316x239 pixel) and a dynamic range of 12-bit. The captured data include the background noise of the infrared focal plane array. An offset correction has been adapted. For the correction 100 frames in a darkened environment were captured to determine the background noise. The mean value of the background noise was determined for each pixel. These results were subtracted from the measured data. The average of 600 measured single shots represents the distribution function (Fig. 3) of the used system.

Furthermore, investigations were done to explore the spatial distribution of the surfaces radiance for various aspect angles of a plate. Consider a plane Lambertian surface which is illuminated by a beam with a cross-section A_r. The angle between the optical axis and the normal of the surface is described by angle φ. The size of the illuminated area A_i is given by $A_r / \cos\varphi$. This relation between irradiance and radiance is depicted in Fig. 4.

The measured 2-d distribution was used to simulate the dependence of the distribution on various aspect angles. A rotation in steps was simulated by scaling the image intensity of the measured 2-d distribution using the cosine function. For the simulation the aspect angle was changed in steps of 15° from $\varphi = -60°$ to $\varphi = 60°$. The results are shown in Fig. 5a. The beam intensity is reduced for an increasing aspect angle of the surface. Corresponding to this simulated dataset a measured dataset was captured. Each distribution was calculated by averaging 600 single shots. The results are shown in Fig. 5b. The beam intensity is reduced for an increasing aspect angle and the shape is distorted.

Figure 4: The irradiance is related to the radiance with the cosine function
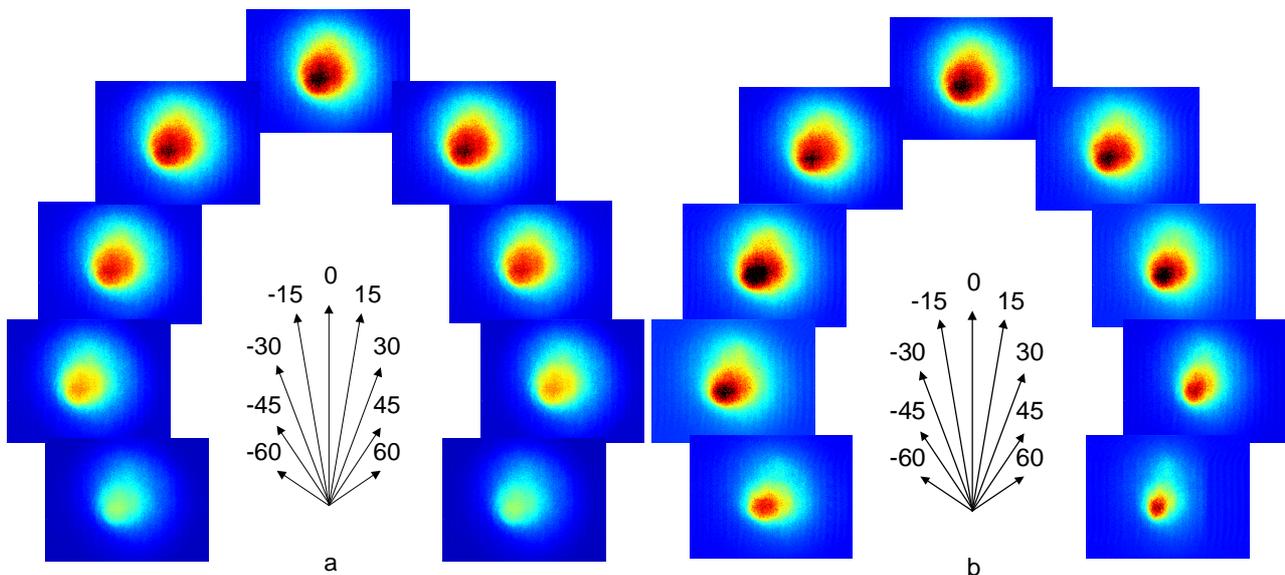
Figure 5: Dependence of the distribution on the aspect angle. a) simulated distributions, b) measured distributions.

4.2 Temporal evaluation

Typically, a change of the surface orientation effects a temporal spread of the pulse. For the temporal evaluation we captured the received pulse. Additionally, the emitted pulse is recorded by using a thin string as reference target, because the emitted pulses vary in form and duration. An example for the measurement of a typical signal which consist of an emitted and a received pulse is shown in Fig. 6.
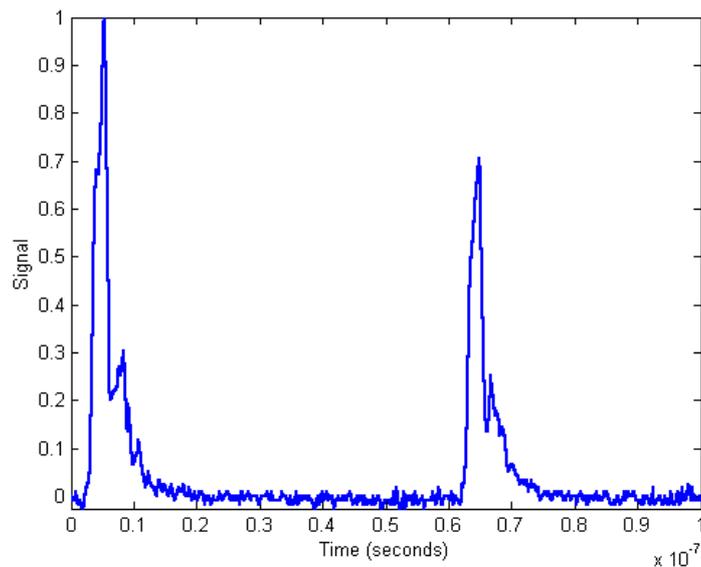
Figure 6: Signal with the emitted and the received pulse.

Pulse width. For investigation of the temporal pulse variation different aspect angles of the plate were examined. The aspect angle was changed in steps of 15° from $\varphi = -75°$ to $\varphi = 75°$. For each angle 100 single shots were emitted and recorded. We determined the pulse widths by FWHM of the emitted and the received pulse. Due to the temporal sampling of the signal the pulse width is calculated by interpolation of adjacent samples. The temporal spread of the signal can be characterized by the difference of the emitted and received pulse width. Fig. 7 shows the measured widths of the emitted and the received pulses in dependence of the aspect angle. Additionally, the difference of both pulse widths is figured. Furthermore the expected difference is shown in Fig. 7 as dotted line. This was simulated considering the beam divergence, the distance, and the aspect angle of the surface.
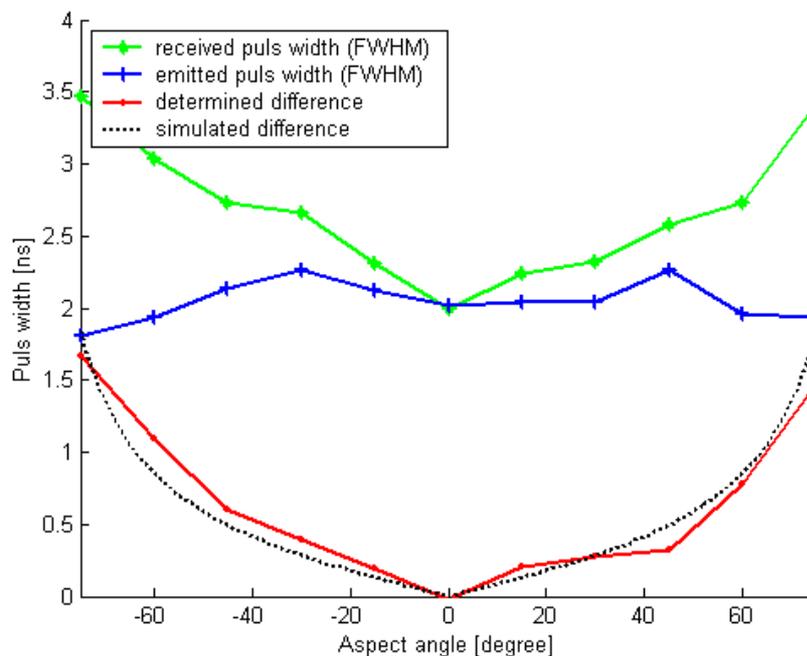
Figure 7: Pulse width and width difference for various aspect angles

Fig. 5 and Fig. 7 show that a variation of aspect angle effects the spatial distribution and the temporal form of signal. The question arise: is it possible to determine the aspect angle from the temporal form of the signal?
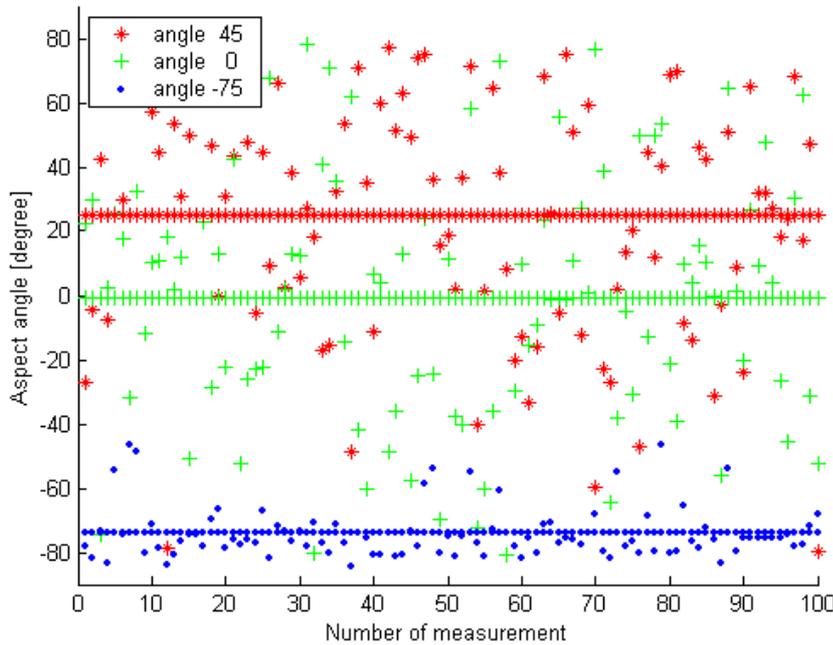
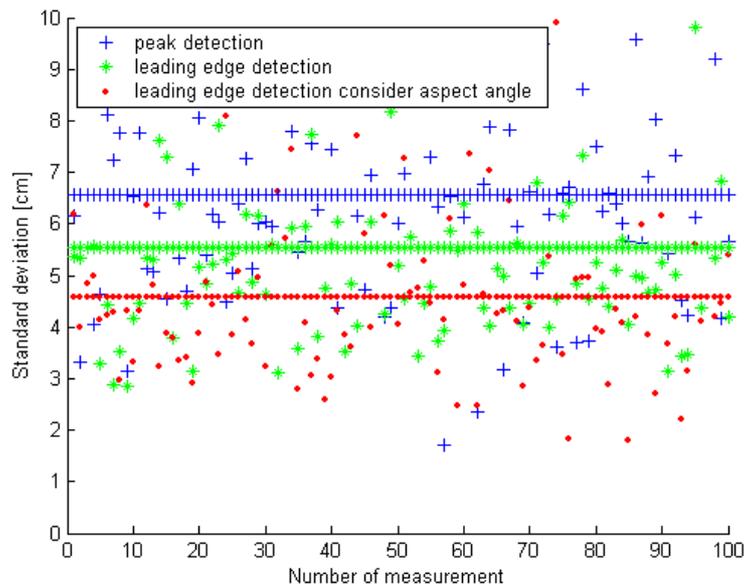| Aspect angle [°]	Mean value [°]	Standard deviation [°]
-75	-74.2	8.2
-60	-63.6	16.4
-45	-42.6	32.1
-30	-29.2	37.3
-15	-15.1	38.9
0	-0.5	40.0
15	15.5	38.7
30	20.9	40.5
45	25.0	38.0
60	49.1	26.9
75	67.3	21.9

Figure 8: Estimation of aspect angles

Table 1: Results of measurements for eleven aspect angles

Estimation of aspect angle. For answering this question single measurements of different aspect angles were examined. From the measured differences of the pulse widths the angles are derived (see dotted line in Fig. 7). Fig. 8 shows the estimated angles from measurements of three different aspect angles of the plate (45 °, 0 °, -75 °). The estimated angles are indicated by different symbols (*, +, .) corresponding to the different aspect angles. In Fig. 8 one can see that the estimated angles for a given aspect angle are scattered for a wide range. A single measurement of an estimated angle does not allow to determine the aspect angle of the surface. For a sample of 100 estimated angles for the same aspect angle the mean value of the angle is calculated. The three mean values are shown as lines in Fig. 8. In contrast to the single estimations the averaged estimation allows to distinguish the three different aspect angles.

The results of the estimation for eleven aspect angles by averaging the measurements are listed in Tab. 1. Furthermore the standard deviation was calculated. A strong variation for each estimated aspect angle is obvious. The mean value of the estimated angles fits to the aspect angle.

Range detection. The yield aspect angle can be used to increase the accuracy of detected range values. Often peak detection or leading edge detection techniques are used for the determination of the range in analog signal processing. For a comparison these techniques are transferred in digital algorithms. Additionally an algorithm was implemented which considers the aspect angle to calculate the range. The peak detection algorithm provides good results for undisturbed peaks of the pulses. If the pulses include noise the peak detection has problems to determine the correct position. For this reason leading edge detection is often used. If we consider surfaces which are not perpendicular to the propagation of the beam, the signal will be spread off and the leading edge may not give the correct central position of the target. Considering the pulse form this allows to correct the systematic error. For this purpose two range values for the emitted and the received pulse are determined at the FWHM threshold. For each signal the range values are averaged and both averaged range values are used to calculate the range.

Figure 9: Standard deviation of the determined range for various detection algorithms

For the evaluation of the three algorithms we measured 100 shots for each of the eleven aspect angles. From this dataset of 1100 measurements we computed the range with the different algorithms. As shown in Tab. 1, the standard deviation depends on the aspect angle. To avoid this dependence each sub-dataset consists of eleven different aspect angles. The standard deviation is calculated for these sub-datasets. These standard deviations of the different algorithms are indicated by the different symbols (+, *, .) and depicted in Fig. 9. The mean value of the standard deviations for each algorithm is plotted as a line.

4.3 Spatio-temporal evaluation

The power of the emitted pulse was weighted with the spatio-temporal beam distribution for a given range. This relation is expressed in Eq. 1. It is difficult to imagine this 4-d distribution of the irradiance $E(r,\varepsilon,\alpha,t)$. Assuming a given range r_1 the spatio-temporal form of $E(r_1,\varepsilon,\alpha,t)$ can be displayed as a spatial 3-d distribution. For that purpose the time t is transformed into an elongation $r_t = t\,c$ with c as speed of light. This spatial 3-d distribution $E(r_1,\varepsilon,\alpha,r_t)$ can be visualized by choosing a threshold E_{th} and displaying the surface of various values from $E_{th}(r_1,\varepsilon,\alpha,r_t)$ (equi-irradiance surface). Surfaces for different irradiances E_{th} with range $r_1 = 50$ m are shown in Fig. 10.
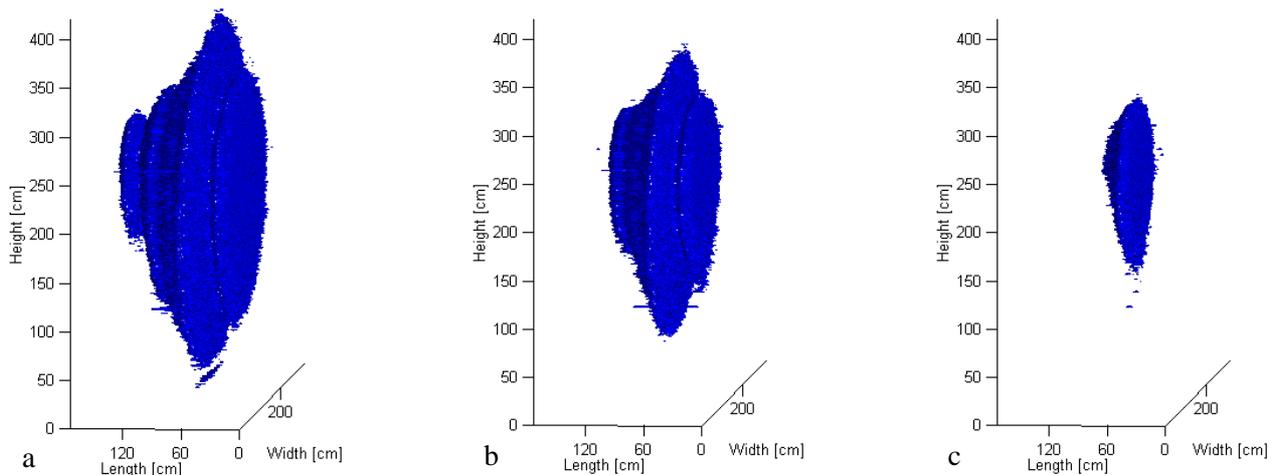
Figure 10: 3-d visualization of equi-irradiance surface. a) $E_{th} = 17$ W/m^2, b) $E_{th} = 25$ W/m^2, c) $E_{th} = 50$ W/m^2

5. DISCUSSION

In the model for the beam propagation we had assumed that the distribution can be described by a symmetric Gaussian distribution (K_t in Eq. 3). But, the measurements of the spatial distribution show an asymmetric distribution (Fig. 3a). This behavior can be observed in Fig. 3b and Fig. 3c. The asymmetric distribution is due to the construction with the flash lamp beside the laser resonator. Especially the distribution in the near field suffers from this distortion. For further theoretical investigations we have to consider special Non-Gaussian distributions. That means, function K_t in Eq. 6 will be described by an array of weighting coefficients. These coefficients were measured (Fig. 3) and used to simulate spatial distribution for various aspect angles (Fig. 5a). The simulated distributions were compared with measured distributions (Fig. 5b). A good similarity of simulated and measured distributions is given for small aspect angles, lets say from $\varphi = -30°$ to $\varphi = 30°$. Above these angles ($\varphi < -30°$ to $\varphi > 30°$) the similarity is less than below. The measured distributions of negative and positive angles are slightly different. The differences can be referred to the anisotropic characteristic of the used material.

For the pulse waveform we have assumed an exponential function (K_l in Eq. 3). An example for an measurement of a real signal containing the emitted and the received pulse can be seen in Fig. 6. The received pulse looks similar, but is attenuated. The waveform of the pulse looks similar to an exponential function, but is distorted by a signal peak with low amplitude and short duration. This peak refers to the fade away of the Raman process of the laser source. Instead of the desirable theoretical delta pulse with its infinite height and zero width we have to handle the real pulse with finite height and width. Emitting a sequence of pulses a strong variation of the pulse width can be observed (Fig. 7, emitted pulse). According to this variation the received pulse width is effected, too. This demands the recording of both, emitted and received pulse for an accurate evaluation. It has been shown that the difference of both pulse widths is less sensitive to pulse variations and can be used for measuring object features. The measured differences fit almost to the expected values, which were calculated assuming optimal conditions (Fig. 7, dotted line). Experiments for estimating the aspect angle of the object surface show a strong variation of the measured angles, but more robust results for the mean value of the measured angles (Fig. 8 and Tab. 1). The accuracy of the measured angle by the mean value yields to very good results ($\Delta\varphi < 5°$) for $\varphi = -75°$ to $\varphi = 15°$, to still good results for $\varphi = 30°$, $\varphi = 60°$, $\varphi = 75°$, and to poor result for $\varphi = 45°$. For an increasing angle φ the standard deviation is decreasing. Low aspect angles show high variation of the angle caused by low variation of the pulse width.

Consideration of the aspect angle allows an improved accuracy for the range detection (Fig. 9). The elimination of the systematic error results in a lower standard deviation of single measurements. The knowledge of temporal and spatial distribution is essential for measuring object features. The visualization of the pulse by a 3-d object which shows spatial together with temporal distributions is very helpful to assess the quality of a pulse. Fig. 10 shows for different ranges two cone-like objects. The base of the cone refers to the leading edge and the corner refers to the decreasing tail of the temporal pulse. A short pulse width shows a small cone height and an obtuse angled corner.

The diameter of the beam is at long range greater than at near range. A large diameter at a sloped surface results in a long temporal spread. For measurement by digital data recording it is advantageous to capture long spread pulses. For digitizing the full waveform a very high data rate would be generated. If we use the given parameters of the experimental system to recording a range interval of 100 m with a spatial resolution of 128x128 samples, we will receive a data volume of 55 Mbytes. A reduction of the data volume is possible by recording the time and only digitizing the area of interest.

6. CONCLUSIONS

In this paper we explored the spatial and the temporal backscattering characteristics of an extended object with simplified surface. For a detailed analysis of the temporal signal form a digitizing receiver unit was essential. Analyzing the signal form of the emitted short duration laser pulse with a FWHM of only a few nanoseconds requires a receiver unit with a bandwidth of some GHz and an appropriate sampling rate. For exploring the capabilities of an airborne system a monostatic bi-directional experimental system was built-up using a fast digitizing receiver unit, and investigations were done on the backscattering characteristic of the received signal form. We modeled the spatio-temporal beam propagation, the spatial reflectance of the surface, and the receiver properties. A time-dependent

description of the received signal power was derived and the special surface property was considered. The investigations considered various aspect angles of a plane surface. We have shown that the estimation of the aspect angle with the received temporal signal is possible. The knowledge of the aspect angle can be used to improve the range detection technique. The 3-d visualization of an equi-irradiance surface allows to assess the spatio-temporal shape of the pulse. To take the temporal waveform into account could be of great interest for future applications.

7. ACKNOWLEDGEMENTS

8. REFERENCES

Abrahamsson S, Brusmark B, Gaunaurd GC, Strifors HC (1991) Target identification by means of impulse radar In: Automatic Object Recognition, SPIE Proc. Vol. 1471: 130-141

Andrews LC, Phillips RL (1998) Laser Beam Propagation through Random Media, SPIE Press, Bellingham, WA

Baltsavias EP, Gruen A, , vanGool L (2001) (eds) Automatic extraction of man-made objects from aerial and space images (III), Lisse: Balkema

Delaye V, Labeye P (2000) High-resolution eye safe time of flight laser range finder, In: Kamerman GW (ed) Laser Radar Technology and Applications V, SPIE Proc. Vol. 4035: 216-225

vanGinnegen B, Stavridi M, Koenderink JJ (1998) Diffuse and specular reflectance from rough surfaces, Applied Optics Vol. 37, No. 1: 130-139

Harms J, Lahmann W, Weitcamp C (1978) Geometrical compression of lidar signals, Applied Optics Vol. 17, No. 7: 1131-1135

Horn BKP, Sjoberg RW (1979) Calculating the reflectance map, Applied Optics Vol. 18, No. 11: 1770-1779

Jelalian AV (1992) Laser Radar Systems, Artec House, Norwood, MA USA

Kamerman GW (1993) Laser Radar, In: Fox CF (ed) Active Electro-Optical Systems, The Infrared & Electro-Optical Systems Handbook, Michigan

Nayar SK, Ikeuchi K, Kanade T (1991) Surface Reflection: Physical and Geometrical Perspectives, IEEE Transactions of Pattern Analysis and Machine Intelligence Vol 13: 611-634, Appendix D

Nicodemus FE, Richmond JC, Hsia JJ, Ginsberg IW, Limperis T (1977) Geometrical Considerations and Nomenclature for Reflectance, NBS Monograph 160, National Bureau of Standards, Washington, D.C.

Oppenheim AV, Schafer RW (1975) Digital Signal Processing, Prentice-Hall Inc., Englewood Cliffs, NJ

Shapiro JH, Reinhold RW, Park D (1986) Performance analyses for peak-detecting laser radars, In: Laser Radar Technology and Applications, SPIE Proc. Vol. 663: 38-56

Steinvall O (2000) Effects of target shape and reflection on laser radar cross sections, Applied Optics Vol. 39, No. 24: 4381-4391

Stilla U, Jurkiewicz K (1999) Reconstruction of building models from maps and laser altimeter data. In: Agouris P, Stefanidis A (eds) Integrated spatial databases: Digital images and GIS. Berlin: Springer, 34-46

Stover JC (1990) Optical Scattering: Measurements and Analysis, SPIE Optical Engineering Press, Bellingham, WA

Torrance KE, Sparrow EM (1967) Theory for Off-Specular reflection From Roughened Surfaces, Journal of the Optical Society of America Vol 57, No 9: 1105-1114

Walker RE, McLean J (1999) Lidar equations for turbid media with pulse stretching, Applied Optics Vol. 38, No. 12: 2348-2397

Wang J, Kostamovaara J (1994) Radiometric analysis and simulation of signal power function in a short-range laser radar, Applied Optics Vol. 33, No. 18: 4069-4076